Microstructure evolution of Ti$_{48}$Zr$_{27}$Cu$_6$Nb$_5$Be$_{14}$ amorphous alloy after semi-solid isothermal treatment

Xin-hua Huang[1, 2], Jing-wen Pu[1], Yong-xin Luo[1], and *Yue-jun Ouyang[2]

1. School of Material, Electricity and Intelligent Manufacturing, Huaihua University, Huaihua 330031, Hunan, China

2. Hunan Renewable Aluminum Innovation Research Center, Huaihua University, Huaihua 330031, Hunan, China

Abstract: The as-cast amorphous Ti$_{48}$Zr$_{27}$Cu$_6$Nb$_5$Be$_{14}$ composites, comprising in situ formed β-Ti ductile crystalline precipitates, were prepared by water cooled copper mold suction casting. Then, the semi-solid composites were obtained after the as-cast composites were treated by semi-solid isothermal treatment. The microstructure evolution and kinetics of the composites were examined. Results show that the microstructures of both the as-cast and semi-solid composites comprise of β-Ti crystal phases and amorphous matrix phases. Before and after treatment, the crystals evolve from fine granular or fine dendritic crystals to coarse crystals. As the treatment temperature increasing or the time prolonging, the average crystal size gradually increases and the surface morphology of the crystals gradually becomes regular. By studying the microstructural evolution and dynamics during the isothermal treatment process, it is found that the final morphology of β-Ti crystals is influenced by the isothermal treatment temperature and time (*t*), and the β-Ti evolution rate increases with an increase in treatment temperature. In addition, a linear relationship was observed between the size of cubic β-Ti crystals (D^3) and *t*; the growth kinetics factor *K* is 3.8 μm^3·s^{-1}. As the *K* value closes to 4 μm^3·s^{-1}, it is inferred the morphology evolution of β-Ti crystals is a coarsening behavior controlled by the diffusion of solute elements.

Keywords: Ti$_{48}$Zr$_{27}$Cu$_6$Nb$_5$Be$_{14}$; amorphous matrix composites; semi-solid; as-cast; microstructure

CLC numbers: TG146.23   **Document code:** A   **Article ID:** 1672-6421(2024)03-287-08

1 Introduction

Amorphous alloys have high strengths and elasticity limits, as well as excellent corrosion resistance and electrical and magnetic conductivity, due to their unique structures. Thus, they have wide application prospects in machinery, electronics, chemicals, sports equipment, and even national defense and military affairs [1-2]. However, their applications as advanced structural materials in engineering are seriously restricted by their highly localized shear behavior, which makes the materials prone to brittle fracture without obvious macroscopic plastic deformation [3-4]. In recent years, amorphous composites have been developed by generating second ductile phases in amorphous matrix, with the aim to improve plasticity. At present, most amorphous composites are obtained by adjusting the composition and controlling the solidification process during cooling [5]. This principle involves that toughness crystals precipitate firstly in the alloy melt, and then the remaining melt forms amorphous matrix. Thus, amorphous composites containing tough crystals and brittle amorphous matrix are obtained.

Commonly, contemporary amorphous composites with varying plastic properties have been prepared by water quenching, arc melting spray casting, and arc melting suction casting [6]. Round rod samples prepared by these methods have surface layers with high amorphous content, while the cores have a large number of crystals. This is because these methods encounter extreme cooling, while the cooling rate along the radial direction of the rod samples is not controllable. In order to avoid this problem, Qiao et al. [7] achieved great success in preparing Zr-based amorphous composites by generating crystals using Bridgman directional solidification. This method could effectively improve

*Yue-jun Ouyang

Male, Ph. D, Professor. Research interests: design and preparation of new alloy materials. He has been responsible for some National Natural Science Foundation Programs and Provincial Natural Science Foundation Projects, obtained 20 invention patents and 10 utility model patents of China. To date, he has published more than 50 academic papers.

E-mail: oyyj0816@163.com

the distribution of the ductile crystals on the cross section of the samples. However, the above mentioned methods allow for the preparation of only simple billets and are not suitable for complex parts. The semi-solid forming method is one of the most promising and precise forming technologies in the 21st century [8-9]. It has unique advantages such as the ability to control the morphology, size, and distribution of precipitates in the alloy melts. Semi-solid forming of amorphous composites is a key technology in the processing and formation of bulk amorphous materials.

The semi-solid isothermal treatment can effectively control solute diffusion, liquid solid interface morphology, and structure homogenization. In addition, the method can reduce solidification shrinkage and internal stress. In recent years, semi-solid treatment processes have been used to treat Zr, Ti and Cu basic amorphous composites for regulating microstructures and improving plasticity [10-12]. The microstructure and mechanical properties of Zr-Ti-Nb-Cu-Be and Ti-Zr-V-Cu-Be system amorphous composites were regulated using similar isothermal treatment processes [13-15]. The $Ti_{44.3}Zr_{35.2}V_{11.8}Cu_{8.1}Be_{2.6}$ composites were treated for thermal insulation treatment, the plasticity was increased from less than 1% to 20% [16]. The $Zr_{56.2}Ti_{13.8}Nb_{5.0}Cu_{6.9}Ni_{5.6}Be_{12.5}$ composites were heated to the liquid-solid two phase (semi-solid) zone for thermal insulation treatment, regulating the microstructure and distribution of the crystals [17]. The compression yield strength and plasticity were determined to be 1,325 MPa and 12.0%, which were 13% and 20% higher than those of the untreated composites, respectively. The results showed that large crystals were obtained after treatment and these coarse crystals improved material's plasticity by generating shear bands. Similarly, for $Zr_{41.2}Ti_{13.8}Cu_{12.5}Ni_{10}Be_{22.5}$ composites, after isothermal treatment, the coarse crystals were obtained and the plasticity increased from 9% to 44%. These coarse crystals can hinder the shear band extension and enhance the plasticity [18]. Based on the semi-solid preform process, Makaya et al. [19] explored the cooling ramp method to prepare $Zr_{66.4}Nb_{6.4}Cu_{10.5}Ni_{8.7}A_{18}$ amorphous composite ingots and found that the forming quality of the ingots was improved. However, the solidification time of the alloy was very short, and the viscosity of the molten metal in the semi-solid temperature range was high, which made it impossible to complete mold filling under suction casting conditions.

Thus, forming bulk amorphous composites by generating crystals in the amorphous matrix in the semi-solid temperature range can be an effective way to address the room temperature brittleness of amorphous alloys. In order to enhance the plasticity, the semi-solid isothermal treatment on $Ti_{48}Zr_{27}Cu_6Nb_5Be_{14}$ amorphous composites was carried out by our group. It was found that the plasticity was greatly improved from 5.3% to 10.2%, with an increase of 92.7%. The main reason is that the treatment changes the crystal morphology and size [20]. However, the crystal evolution behavior and mechanism during the treatment have not been revealed. This study focuses on the evolution and growth kinetics of β-Ti crystals for $Ti_{48}Zr_{27}Cu_6Nb_5Be_{14}$ amorphous composites during semi-solid isothermal treatment.

2 Experimental procedure

Pure metal components Ti (99.95%), Zr (99.96%), Nb (99.93%), Cu (99.95%), and Be (99.92%) were used proportionately to obtain an alloy of $Ti_{48}Zr_{27}Cu_6Nb_5Be_{14}$ with a molar ratio. Alloy ingots were melted in a high-vacuum (10^{-4} Pa) arc melting furnace under high-purity Ar. The $Ti_{48}Zr_{27}Cu_6Nb_5Be_{14}$ ingots were melted 4–5 times to ensure chemical homogeneity, and then, they were cast using suction casting with a water cooled copper mold to obtain cylindrical samples with a diameter of 4 mm and length of 70 mm. In this way, the as-cast samples of $Ti_{48}Zr_{27}Cu_6Nb_5Be_{14}$ amorphous composites were obtained.

Then, the as-cast samples were subjected to semi-solid isothermal treatment, which consisted of three main steps: First, the as-cast samples were vacuum encapsulated in quartz tubes. Second, the electric furnace (YFFG40/13G-YC) was heated to semi-solid temperature in advance, and then the packaged samples were put into the furnace to hold for a certain period of time. Third, the samples were removed from the furnace and then immediately water quenched. The semi-solid samples, a diameter of 4 mm and length of 30 mm, were prepared after these processes. The main process flow of these steps is shown in Fig. 1.

Based on the above treatment process, four groups of semi-solid samples were prepared at 750, 800, 850 and 900 °C with the holding time of 30 min. Another six groups of semi-solid samples were prepared at 850 °C for 1, 3, 5, 10, 20 and 40 min, respectively.

The phase constitution of the as-cast and semi-solid amorphous composite samples was analyzed using D8 Advance X-ray diffraction (XRD, Cu Kα). The microstructure was observed and analyzed by a Qaunta 200F scanning electron microscope (SEM) and Digital Micrograph 3.4 software. The image analysis software Image Pro Plus 6.0 (IPP6.0) was used to quantitatively analyze the volume fraction (φ) of crystal phases, the equivalent crystal size (D), and the shape factor (S_F) using Eqs. (1)–(3), respectively:

$$\varphi = \frac{\sum_{i=1}^{N} A_i}{A} \tag{1}$$

$$D = \frac{\sum_{i=1}^{N} \sqrt{4A_i/\pi}}{N} \tag{2}$$

$$S_F = \frac{\sum_{i=1}^{N} \left(4\pi A_i / P_i^2\right)}{N} \tag{3}$$
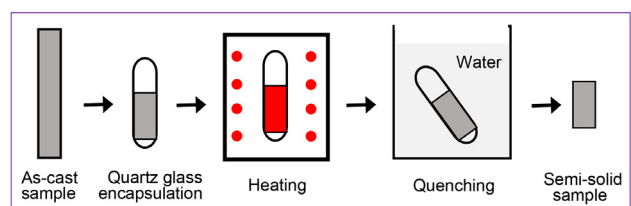

Fig. 1: Schematic diagram of the main process flow of semi-solid isothermal treatment

where A_i is the area of the ith grain, P_i is the circumference of the ith grain, A is the field area, and N is the number of grains to be measured.

3 Results and discussion

3.1 Microstructures of as-cast samples

The microstructures and phase constitution of the as-cast $Ti_{48}Zr_{27}Cu_6Nb_5Be_{14}$ amorphous composite samples are shown in Figs. 2(a) and (b). XRD analysis shows that the existence of amorphous phase and bcc β-Ti crystals. Thus, the as-cast microstructure is composed of amorphous and β-Ti crystal phases. The composition of β-Ti crystals and amorphous phases was examined using EDS, and the results are shown in Fig. 2(d). It is found that the content of solvent atom Ti is higher in crystals than in amorphous, and there is a solubility difference.

The β-Ti crystals are distributed uniformly in the amorphous matrix, and the length of the primary dendrite arm ranges from a few micrometers to several tens of micrometers. The volume fraction of β-Ti crystals is approximately 61%, as determined using IPP6.0 software. Element Nb with a high melting point plays two main roles in the formation of the microstructures of the as-cast amorphous composites [12]. On the one hand, Nb promotes β-Ti crystals formation and increases the number of crystals within the amorphous matrix. On the other hand, Nb makes it difficult for the atoms in the remaining melt to diffuse, so it limits crystal growth and leads to fine crystals. During the solidification process, the main elements Ti, Zr, and Nb nucleate in the form of solid solutions and the nuclei grow as dendrites. Because of rapid cooling, these dendrites can not grow up in time and instead form fine dendrites. The remaining solution forms amorphous matrix.

3.2 Influence of semi-solid isothermal treatment on microstructures of $Ti_{48}Zr_{27}Cu_6Nb_5Be_{14}$ alloy

3.2.1 Effect of semi-solid isothermal treatment temperature on microstructure

Figure 3 shows the XRD profiles of the semi-solid samples obtained at 750, 800, 850, and 900 °C for 30 min. The diffuse peaks with typical amorphous characteristics are superimposed with sharp diffraction peaks corresponding to the β-Ti crystals. The samples still comprise of β-Ti crystals and amorphous phases after semi-solid isothermal treatment. Thus, the isothermal treatment does not change the phase constitution.

Figures 4(a)–(d) represent the microstructures of the samples after heat treatment at 750, 800, 850, and 900 °C for 30 min, respectively. For the semi-solid samples obtained after treatment at 750 °C for 30 min, the crystal morphology is no longer dendritic as that of as-cast sample. The ductile phases in the semi-solid samples mainly consist of slender curved stripped β-Ti crystals, along with a small amount of short stripped crystals and granular crystals; the crystal morphology is irregular, and some strip crystals are connected to each other, as shown in Fig. 4(a). Compared to 750 °C, when T=800 °C, the lengths of the β-Ti crystals become shorter, the radial sizes are larger, and the crystal curvature are smaller. The β-Ti crystals are mainly stripped and granular, as shown
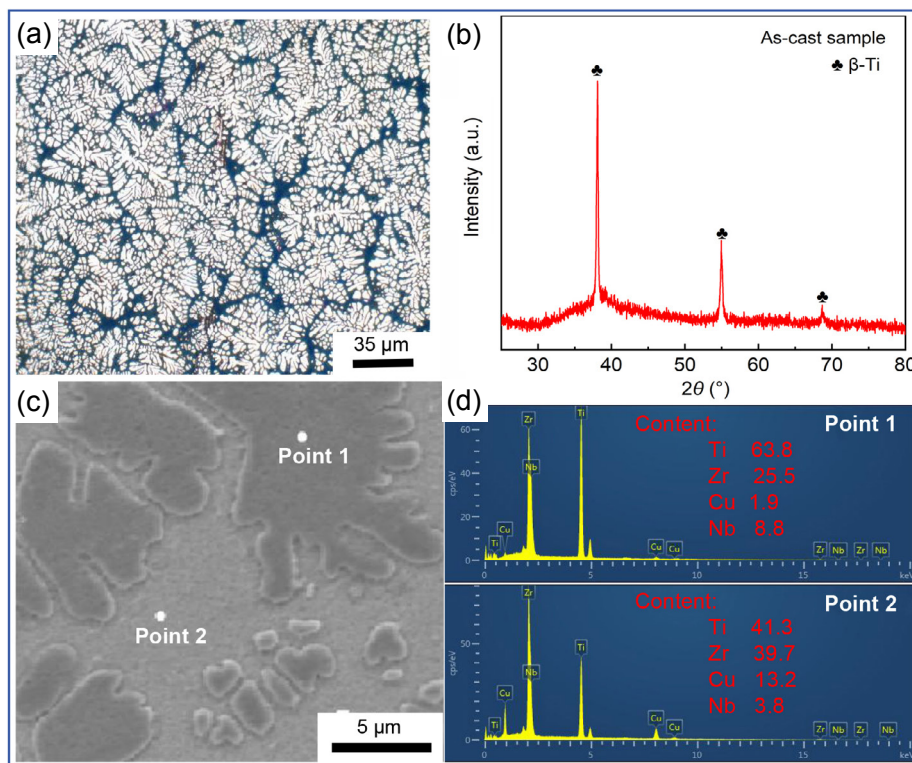

Fig. 2: Microstructures of as-cast $Ti_{48}Zr_{27}Cu_6Nb_5Be_{14}$ alloy produced by copper mold suction casting: (a) optical microstructure; (b) XRD pattern; (c) selected points for composition analysis; (d) EDS analysis of selected points

in Fig. 4(b). As treatment temperature increases to 850 °C, the radial size of the rod-shaped crystals increases, and the crystal length and curvature still decrease. Thus, at 850 °C, the morphology of crystals is mainly characterized by short, coarse rod-shaped structures, with a few crystals exhibiting a near-spherial morphology, as shown in Fig. 4(c). Finally, when T= 900 °C, the surfaces of the near-spherical crystals are more rounded and closer to spherical, and the rod-shaped crystals have shorter lengths and larger radial dimensions than those of specimens treated at 850 °C, as shown in Fig. 4(d). It can be seen that as the temperature increases from 750 °C to 900 °C, the crystals evolve from slender curved stripped crystals to long rod-shaped crystals, then to short coarse rod-shaped crystals, and finally to nearly spherical crystals. It shows that the surface morphology of the crystals gradually becomes regular,
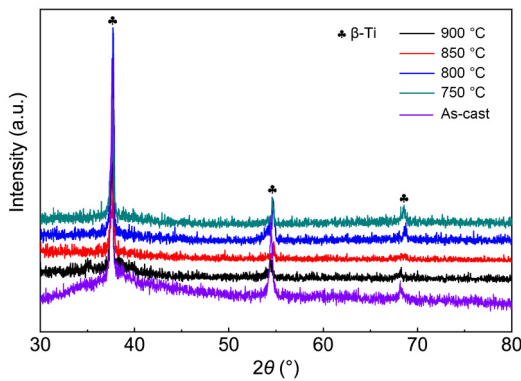
and the crystal size also increases gradually.

The significant change from dendrites to stripped crystals occurs as the secondary dendrite arms peel from the dendrites during the semi-solid isothermal treatment process. In contrast, the adjacent secondary dendrite arms that peel off merged and coarsen with each other, evolving into short stripped crystals. Furthermore, as the dendrite arms peel off from the dendrite, the crystal morphology changes from dendritic to trunk, resulting in the crystals evolving from dendrites to trunk crystals. Moreover, the adjacent trunk crystals are connected to each other, resulting in the formation of long curved stripped crystals. A small amount of granular crystals evolve from partially detached dendritic arms by growing and rounding.

The relationship curves among the volume fractions and shape factor and treatment temperatures were plotted, as shown in Fig. 5. As the treatment temperature increases, the β-Ti crystal volume fraction decreases, which implies that the content of β-Ti crystals decreases. This is because the solvent Ti atom is the crystal forming element, and its concentration in the crystals is much higher than that in the amorphous phases [21]. During the semi-solid isothermal treatment, solvent Ti atoms diffuse from the crystals to the amorphous matrix. With an increase in treatment temperature, the diffusion coefficient increases, which accelerates the diffusion of atoms. These mean that more crystals disappear due to the disorder of atomic spatial arrangement caused by the diffusion of atoms. In contrast, for shape factor, it gradually increases with an increase in temperature. In conclusion, the content and morphology of the β-Ti crystals are considerably influenced by the treatment temperature.

Fig. 3: XRD test results of semi-solid samples after treatment at 750, 800, 850, and 900 °C for 30 min and as-cast samples
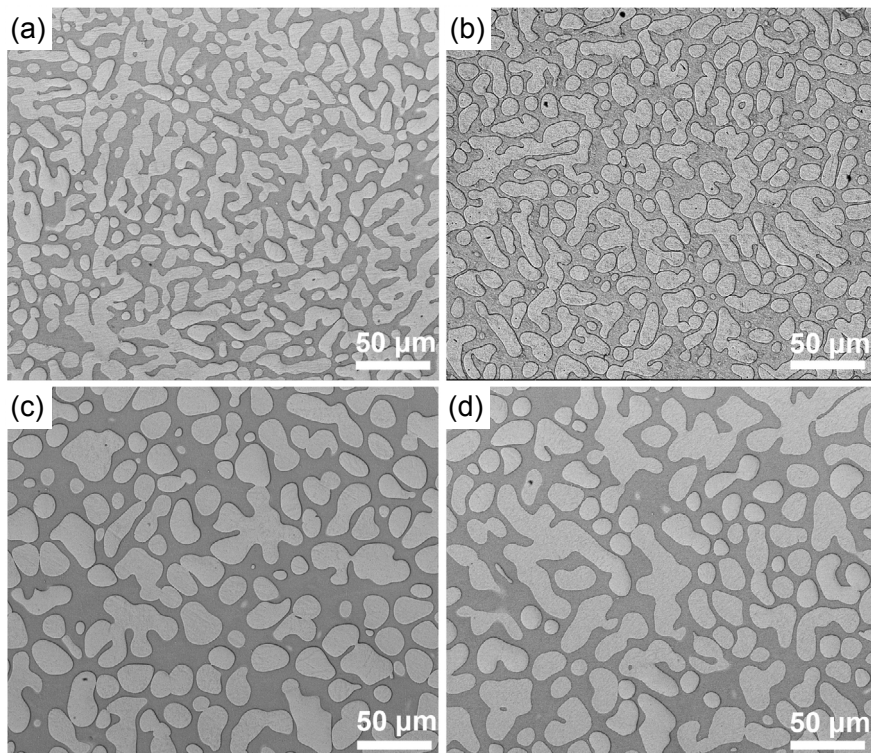

Fig. 4: Evolved microstructures produced after remelting and isothermal holding for 30 min at different temperatures: (a) 750 °C; (b) 800 °C; (c) 850 °C; (d) 900 °C
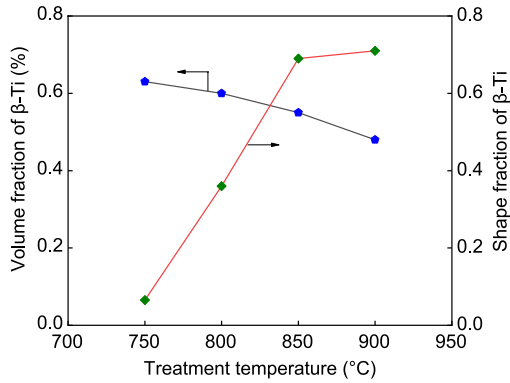
Fig. 5: Effects of isothermal holding temperature on shape factor and fraction solid of β-Ti phase of $Ti_{48}Zr_{27}Cu_6Nb_5Be_{14}$ alloy

When the treatment temperature increases from 750 °C to 900 °C, the slender curved crystals evolves into short and thick rod-shaped crystals, and it is manifested by a decrease in length and increase in radial size, i.e., a smaller length to diameter ratio. Irregular crystals evolve into crystals with higher shape fraction, and they gradually become more rounded. The shape factor of the β-Ti crystals increases from 0.06 to 0.69, as shown in Fig. 5, with an increase in temperature from 750 °C to 900 °C. Meanwhile, the distribution of β-Ti crystals gradually becomes sparse and the crystal size becomes greater as the increase of temperature. The quantitative analysis shows that the volume fractions of the β-Ti crystals decrease as the temperature increases from 750 °C to 900 °C. Thus, a higher treatment temperature results in more favorable changes in the morphologies and sizes of crystals.

3.2.2 Effect of semi-solid isothermal treatment time on microstructure

The phase constitutions of semi-solid samples, after isothermal treatment at 850 °C for 1, 3, 5, 10, 20 and 40 min, are shown in Fig. 6. The phases of the semi-solid samples are still β-Ti crystal and amorphous phase, which indicates the holding time do not change the phase constitution of the composite. The microstructure evolutions of β-Ti crystals of the semi-solid samples after isothermal treatment at 850 °C at different treatment durations are shown in Fig. 7. Based on the statistical data counted from Fig. 7 by IPP6.0 software, quantitative analysis was carried out using Eq. (1). The β-Ti crystal volume fractions of the semi-solid samples treated at 850 °C for 1 and 3 min are 61.4% and 57.2%, respectively. With further increase in holding time from 5 to 40 min, the volume fractions are 56.8%, 56.2%, 55.7% and 55.3%, respectively. It can be seen that the values change very little with further extension of time, which indicates that the sample state is in equilibrium.

After holding at 850 °C for 1 min, the secondary arms of the β-Ti dendrites are obviously coarsened, and the dendritic morphologies of the crystals are no longer obvious, comparing to the dendrites of the as-cast samples. Most of the secondary
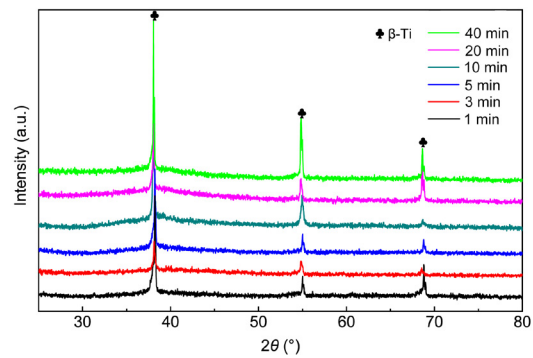

Fig. 6: XRD patterns of semi-solid $Ti_{48}Zr_{27}Cu_6Nb_5Be_{14}$ samples treated at 850 °C for 1, 3, 5, 10, 20, and 40 min
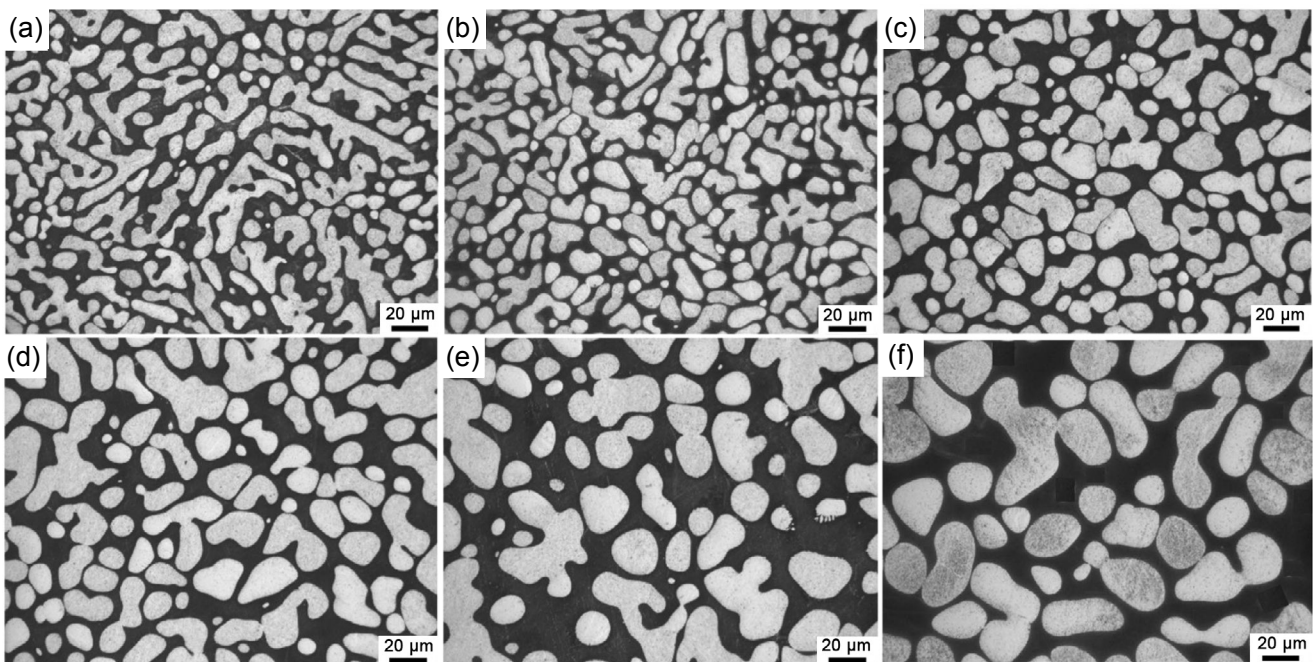

Fig. 7: Evolution of β-Ti phase during isothermal holding at 850 °C for different durations: (a) 1 min; (b) 3 min; (c) 5 min; (d) 10 min; (e) 20 min; (f) 40 min

dendrite arms are separated from the dendrites by fusing, as shown in Fig. 7(a). At holding time of 3 min, dendritic-shaped crystals disappear, the β-Ti crystals evolve into short coarse rod-shaped crystals, as shown in Fig. 7(b). With further increase in holding time, the fine particles gradually disappear, the number of coarse particles increases, thus, the average crystal size also increases. What's more, their surface morphology gradually becomes more uniform, and rod-shaped crystals eventually evolve into nearly spherical or spherical crystals, the average crystal size also increases, as shown in Figs. 7(b) to (f). The above analysis shows that the treatment time mainly affects the β-Ti crystal morphology and size when the treatment temperature is constant.

To further describe the characteristic changes of the β-Ti crystals, the characteristic parameters of the crystal were analyzed, as shown in Fig. 8. It shows the relationship between the shape factors and average equivalent size of the β-Ti crystals and holding time. With an increase in treatment time, the average crystal size increases, which coincides with the phenomena observed in metallographic diagram in Fig. 7. Compared with the dendrites in the as-cast samples, when the holding time is less than 5 min, with the increase of holding time, the shape factor and grain size of the crystals increase rapidly, and this increasing trend becomes gentler when treatment time is more than 5 min.
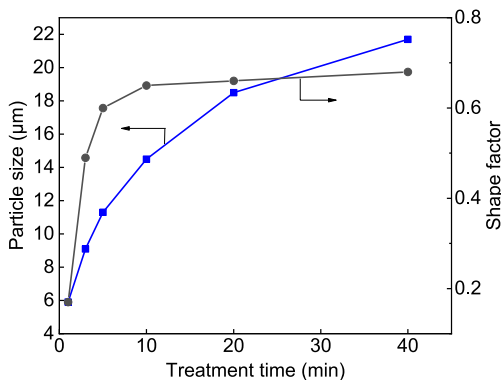

Fig. 8: Effects of isothermal holding time interval on shape factor and particle size of β-Ti phase

3.3 Crystal growth kinetics during treatment

As mentioned in Section 3.2.2, with increase in semi-solid isothermal treatment time, the crystal β-Ti size and morphology change significantly. Therefore, the reasons for the changes should be discussed and analyzed.

During the semi-solid isothermal treatment, the growth and spheroidization of the β-Ti crystals are spontaneous processes driven by interfacial energy [22]. Similarly, crystal changes in conventional aluminum-magnesium alloys during treatment are driven by interfacial energy [23-24]. So, according to the curve relationship and the general expression between grain size D and treatment time t, the growth kinetics during semi-solid isothermal treatment are described by Eq. (4) [25-26]:

$$D^n - D_0^n = Kt \qquad (4)$$

where D_0 is the initial crystal size, n is the crystal growth index, and K is the growth kinetics factor. With time t as the variable, the derivative function equation is obtained by determining the derivative for Eq. (4), and then, the logarithmic functional equation is obtained by taking the logarithm on both sides of the derivative functional equation, as shown in Eq. (5):

$$\lg\frac{\mathrm{d}D(t)}{\mathrm{d}t} = -(n-1)\lg D(t) + \lg K - \lg n \qquad (5)$$

Based on the quantitative analysis results from Figs. 5 and 8, $\lg[D(t)]$ is defined as the independent variable, and $\lg[\mathrm{d}D(t)/\mathrm{d}t]$ is the variable, serving as horizontal and vertical coordinates, respectively. The linear relationship between $\lg[\mathrm{d}D(t)/\mathrm{d}t]$ and $\lg[D(t)]$ is plotted, and $-(n-1)$ is the slope of the straight line, according to Eq. (5), the result is shown in Fig. 9. Thereafter, the β-Ti crystal growth index $-(n-1)=-2.6$ or $n=3.6$ is obtained when variance $R^2=0.996$ by using the linear fitting.
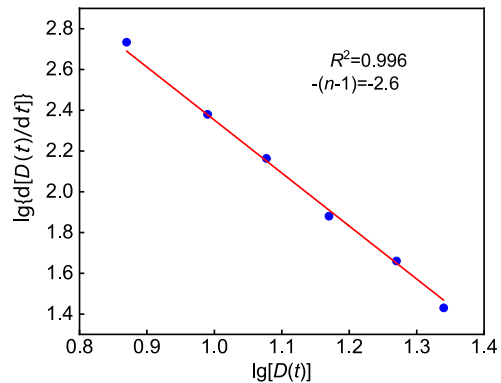

Fig. 9: Calculation of slope value n of straight linear relationship between $\lg[D(t)]$ and $\lg\{\mathrm{d}[D(t)/\mathrm{d}t]\}$ in $Ti_{48}Zr_{27}Cu_6Nb_5Be_{14}$ amorphous composites isothermally held at 850 °C

According to the classical crystal growth mechanism, when the crystal growth index $n=2$, the crystal growth process comprises the curvature driven migration of crystal boundaries; at $n=3$, solute atoms diffuse across crystal boundaries, and at $n=4$, the crystal growth process is controlled by lattice diffusion [27]. Therefore, during semi-solid isothermal treatment, the growth behavior of the β-Ti crystals conforms to the Lifshitz-Slyozov-Wagner (LSW) model, that is, the growth process of the β-Ti crystals is a coarsening behavior controlled by the diffusion of solute atoms and lattice diffusion [28-30]. According to Eq. (4), the cubic size (D^3) of the β-Ti crystal diameters at 850 °C and treatment time t are linearly regressed [31-32]. A good linear relationship between D^3 and t is obtained, as shown in Fig. 10, which further indicates that the growth behavior of the β-Ti crystals during semi-solid isothermal treatment conforms to the LSW model. According to the linear relationship (Fig. 10), the β-Ti crystal growth kinetics factor $K=3.8$ $\mu m^3 \cdot s^{-1}$ is calculated at variance $R^2=0.997$ during linear fitting.

The growth kinetics factor K of the β-Ti crystals is influenced by the thermophysical properties of the materials [33], such as
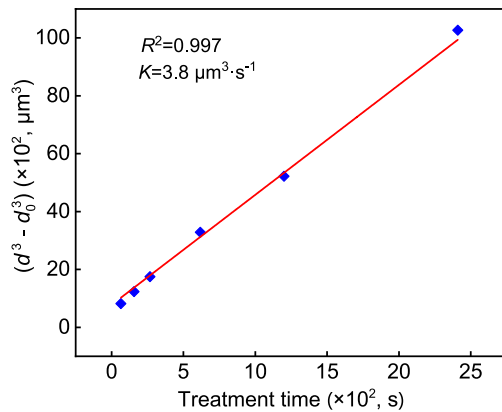
Fig. 10: Relationship between isothermal holding time interval and cubic particle size of β-Ti phase at isothermal holding temperature of 850 °C

diffusion coefficient and interface energy. A smaller K implies a smaller diffusion coefficient. The diffusion coefficient is closely related to the viscosity of the liquid. A small K value also indicates a high viscosity of the liquid. The high viscosity and low diffusion coefficient of the molten metal make it difficult for atoms to migrate and diffuse, which in turn makes it challenging for them to arrange in an orderly manner, resulting in strong amorphous formation ability. Molten amorphous of the $Ti_{48}Zr_{27}Cu_6Nb_5Be_{14}$ composite exhibit a tendency to crystallize when the temperature decreases during water quenching. The small ordered atomic clusters during the incubation period are unable to nucleate and grow due to their low K values and high liquid viscosity, making it difficult for atoms to diffuse, resulting in no crystallization. This is why the β-Ti crystal volume fraction does not increase after the semi-solid isothermal treatment.

In summary, by regulating the isothermal treatment temperature and time, the variation rules of the microscopic features such as crystal size, volume fraction, and surface morphology were analyzed. Then, the evolutionary processes of the β-Ti crystal morphology were revealed, with time extending or temperature increasing. In addition, by calculating n and K, it reveals that the evolution of the crystal morphology is driven by the interfacial energy and the concentration of solvent atoms. These reveal the evolution mechanism of the crystals during isothermal treatment, which provides a theoretical basis for the regulation of crystal shape and size.

4 Conclusions

(1) Semi-solid isothermal treatment does not influence the phase constitution of the $Ti_{48}Zr_{27}Cu_6Nb_5Be_{14}$ amorphous composites. The microstructures of the as-cast and semi-solid samples comprise β-Ti crystals and amorphous phases.

(2) Increasing with treatment temperature or time, the β-Ti dendrites in as-cast state evolve into slender curved strip crystals, then to short coarse rod-shaped crystals, and eventually to nearly spherical or spherical crystals.

(3) The semi-solid isothermal treatment temperature and treatment duration determine the final morphologies of the β-Ti crystals. The growth behavior of the β-Ti crystals conforms to the LSW model, and it has the same microstructure evolution mechanism as that of traditional aluminum and magnesium alloys.

Conflict of interest

The authors declare that they have no conflict of interest.

References

[1] Inoue A, Takeuchi A. Recent development and application products of bulk glassy alloys. Acta Materialia, 2011, 59(6): 2243–2267.

[2] Gao X F, Ge N, Dong F Y, et al. Deformation and fracture of a Zr-Al-Cu metallic glass ribbon under tension near glass transition temperature. China Foundry, 2018, 15(3): 216–221.

[3] Lu Y Z, Su S, Zhang S B, et al. Controllable additive manufacturing of gradient bulk metallic glass composite with high strength and tensile ductility. Acta Materialia, 2021, 206: 116632.

[4] Shan S F, Wang H, Zhang B, et al. Influence of niobium and yttrium on plastic deformation energy and plasticity of Ti-based amorphous alloys. China Foundry, 2021, 18(1): 60–67.

[5] Liu S Y, Dhiman A, Shin Y C, et al. In-situ synthesis of Zr-based bulk metallic glass composites with periodic amorphous-crystalline microstructure for improved ductility via laser direct deposition. Intermetallics, 2019, 111: 106503.

[6] Hays C C, Kim C P, Jonhson W L. Microstructure controlled shear band pattern formation and enhanced plasticity of bulk metallic glasses containing in situ formed ductile phase dendrite dispersions. Physical Review Letters, 2000, 84(13): 2901–2904.

[7] Qiao J W, Wang S, Zhang Y, et al. Large plasticity tensile necking of Zr-based bulck-metallic-glass-matrix composites synthesized by Bridgman solidification. Applied Physics Letter, 2009, 94(15): 151905.

[8] Guan R G. Theories and techniques of semi-solid metal processing. Beijing: Metallurgical Industry Press, 2005. (In Chinese)

[9] Wang W H. The nature and properties of amorphous matter. Progress in Physics, 2015, 33: 177–351. (In Chinese)

[10] Zhang H, Wang Z, Yang H J, et al. A flow model in bulk metallic glasses. Scripta Materialia, 2023, 222(1): 115047.

[11] Hofmann D C, Roberts S N, Kozachkov H. Infrared thermal processing history of a Ti-based bulk metallic glass matrix composite manufactured via semi-solid forging. Acta Materialia, 2015, 95: 192–200.

[12] Inoue A, Kong F L, Zhu S L, et al. Production methods of engineering glassy alloys and composites. Intermetallics, 2015, 58: 20−30.

[13] Hofmann D C, Suh J Y, Wiest A, et al. Designing metallic glass matrix composites with high toughness and tensile ductility. Nature, 2008, 451: 1085−1089.

[14] Hofmann D C, Suh J Y, Wiest A, et al. Development of tough, low-density titanium-based bulk metallic glass matrix composites with tensile ductility. Proceedings of the National Academy of Sciences, 2008, 105(51): 20136−20140.

[15] Hofmann D C, Suh J Y, Wiest A, et al. New processing possibilities for highly toughened metallic glass matrix composites with tensile ductility. Scripta Materialia, 2008, 59(7): 684−687.

[16] Hofmann D C, Kozachkov H, Khalifa H E, et al. Semi-solid induction forging of metallic glass matrix composites. Journal of the Minerals Metals and Materials Society, 2009, 61(12): 11−17.

[17] Sun G Y, Chen G, Chen G L. Comparison of microstructures and properties of Zr-based bulk metallic glass composites with dendritic and spherical BCC phase precipitates. Intermetallics, 2007, 15(5): 632−634.

[18] Xiang Q C, Feng Z B, Zhang W, et al. Effect of infiltrating time on interfacial reaction and properties of tungsten particles reinforced Zr-based bulk metallic glass composites. China Foundry, 2020, 17(4): 253−259.

[19] Makaya A, Tamura T, Miwa K. Cooling slope casting process for synthesis of bulk metallic glass based composites with semisolid structure. Metallurgical and Materials Transactions: A, 2010, 41(7): 1646−1657.

[20] Huang X H, Zhu L H, Guo H M, et al. Shear bands of as-cast and semi-solid $Ti_{48}Zr_{27}Cu_6Nb_5Be_{14}$ bulk metallic glass matrix composites. China Foundry, 2021, 18(1): 75−82.

[21] Park J M, Lim K R, Park E, et al. Internal structural evolution and enhanced tensile plasticity of Ti-based bulk metallic glass and composite via cold rolling. Journal of Alloys and Compounds, 2014, 615: S113−S117.

[22] Marsh S P, Glicksman M E. Overview of geometric effects on coarsening of mushy zones. Metallurgical and Materials Transactions: A, 1996, 27: 557−567.

[23] Wang H, Davidson C J, Stjohn D H. Semisolid microstructure evolution of AlSi7Mg alloy during partial remelting. Materials Science and Engineering: A, 2004, 368: 159−167.

[24] Khalifa W, Tsunekawa Y, Okumtya M. Effect of reheating to the semisolid state on the microstructure of the A356 aluminum alloy produced by ultrasonic melt-treatment. Solid State Phenomena, 2008, 141: 499−504.

[25] Lu Z, Hu X, Li Y. Thermodynamics of La based La-Al-Cu-Ni-Co alloys studied by temperature modulated DSC. Intermetallics, 2000, 8(5): 477−480.

[26] Debenedetti P G, Stillinger F H. Supercooled liquids and the glass transition. Nature, 2001, 410(6825): 259−267.

[27] Lu L, Tao N R, Wang L B, et al. Grain growth and strain release in nanocrystalline copper. Journal of Applied Physics, 2001, 89(11): 6408 −6414.

[28] Lifshitz I M, Slyozov V V. The kinetics of precipitation from supersaturated solid solutions. Journal of Physics and Chemistry of Solids, 1961, 11: 35−50.

[29] Umantsev A, Olson G B. Ostwald ripening in multicomponent alloys. Scripta Materialia, 1993, 29: 1135−1140.

[30] Semiatin S L, Kirby B C, Salishchev G A. Coarsening behavior of an alpha-beta titanium alloy. Metallurgical and Materials Transactions: A, 2004, 35(9): 2809−2819.

[31] Lifshttz I M, Slyozov V V. The kinetics of precipitation from supersaturated solid solutions. Journal of Physics and Chemistry of Solids, 1961, 11: 35−50.

[32] Cui J, Liu Y, Liu S. Internal friction behavior of $Ti_{48}Zr_{20}Nb_{12}Cu_5Be_{15}$ metallic glass composite. Rare Metal Materials and Engineering, 2022, 51(5): 1637−1642.

[33] Zhang W, Xiang Q C, Qu Y D, et al. Effect of melt cooling rate on glass transition kinetics and structural relaxation of Vit1 metallic glass. China Foundry, 2021, 18(2): 118−123.